Journal of Materials Chemistry A

ROYAL SOCIETY OF CHEMISTRY

PAPER

View Article Online
View Journal | View Issue



Cite this: J. Mater. Chem. A, 2023, 11, 12846

# Interdiffused thermoplastic urethane-PEDOT:PSS bilayers with superior adhesion properties for high-performance and intrinsically-stretchable organic solar cells†

Jinho Lee,‡[a] Jin-Woo Lee,‡[a] Hyunggwi Song,[b] Myoung Song,[b] Jinseok Park,[a] Geon-U Kim,[a] Dahyun Jeong,[a] Taek-Soo Kim[b] and Bumjoon J. Kim *[a]

Despite the rapid increases in the performance of intrinsically-stretchable organic solar cells (IS-OSCs), both the power conversion efficiency (PCE) and stretchability of the IS-OSCs should be further enhanced for their use in wearable electronics. Here, we realize efficient (PCE = 13.1%) and highly stretchable (strain at $PCE_{80\%}$ = 34%) IS-OSCs by developing a stretchable substrate-bottom electrode made of a molecular interdiffusion (MID)-assisted thermoplastic urethane-poly(3,4-ethylenedioxythiophene):poly(styrenesulfonate) (TPU-PEDOT:PSS) bilayer. The interdiffused bilayer in the MID-based TPU-PEDOT:PSS affords a strongly adhesive interface with fracture energy ($G_c$) = 45.0 J $m^{-2}$, which is 3-times higher than the conventional stamp-transferred (ST) TPU-PEDOT:PSS ($G_c$ = 15.1 J $m^{-2}$). Importantly, the increased adhesion of MID-based TPU-PEDOT:PSS significantly enhances the overall IS-OSC durability. For example, the stretchability of the MID-based IS-OSCs (strain at $PCE_{80\%}$ = 34%) was 2-times higher than the conventional ST-based IS-OSCs (strain at $PCE_{80\%}$ = 17%) when the active layer was PM6:Y6-BO:N2200. The finite element simulation observes that the high adhesion between the TPU and PEDOT:PSS layers effectively dissipates mechanical stress and prevents cracking at their interface, enhancing the stretchability of the entire IS-OSCs. Therefore, our work provides a useful strategy for developing stretchable transparent electrodes and demonstrates the importance of their interfacial adhesion properties in achieving efficient and highly stretchable IS-OSCs.

Received 19th December 2022
Accepted 13th April 2023

DOI: 10.1039/d2ta09874a

rsc.li/materials-a



**10th anniversary statement**

Congratulations on the 10th anniversary of the publication of *Journal of Materials Chemistry A*. *Journal of Materials Chemistry A* has made significant contributions to advancing material technologies for energy and sustainability. Over the years, we have been honored to publish various research results in the *Journal of Materials Chemistry A*, focusing on developing materials for efficient photovoltaic devices, stretchable electronic devices, as well as eco-friendly device fabrication processes. Examples of our contributions to the journal can be found: starting from *J. Mater. Chem. A*, 2013, 1, 14538 (our first contribution) to *J. Mater. Chem. A*, 2022, 10, 20312 (most recent contribution). Additionally, it has been an honor and a pleasure for us to serve the journal in different roles as authors, reviewers, and advisory board members. Building upon its successful leadership in the area of materials chemistry for the past ten years, we expect and believe that Journal of Materials Chemistry A will continue to represent diverse and ground-breaking research topics related to materials chemistry. We believe that Journal of Materials Chemistry A will continue its success and maintain its prominence and dominance in the next decades and beyond.

## 1. Introduction

Intrinsically stretchable organic solar cells (IS-OSCs), in which all the consisting layers are stretchable, have recently emerged as a promising wearable power source.[1–3] While various high-performance IS-OSCs have been developed in the past years,[4–17] their stretchability should be further improved to meet the large tensile strain required for the human body movements in wearable applications (*i.e.*, ~50% strain at human joints or elastic skins).[18,19] To this end, researchers have focused on developing photoactive materials to improve the mechanical robustness of the high-performance IS-OSCs.[13,20–27] For example, Wang *et al.* incorporated 5 wt% of trimethylsiloxy-terminated polydimethylsiloxane (PDMS) elastomers into PTB7-Th:IEICO-

[a]Department of Chemical and Biomolecular Engineering, Korea Advanced Institute of Science and Technology (KAIST), Daejeon 34141, Republic of Korea. E-mail: bumjoonkim@kaist.ac.kr

[b]Department of Mechanical Engineering, Korea Advanced Institute of Science and Technology (KAIST), Daejeon 34141, Republic of Korea

† Electronic supplementary information (ESI) available. See DOI: https://doi.org/10.1039/d2ta09874a

‡ These authors contributed equally to this work.

4F-based active layer, and demonstrated highly stretchable IS-OSCs retaining 87% of the initial power conversion efficiency (PCE) at 20% of strain.[20] In addition, our group demonstrated IS-OSCs with a high PCE (12.73%) and stretchability (strain at $PCE_{80\%} = 32\%$) by developing a series of conjugated polymers containing hydrogen-bonding capable units.[14] Nonetheless, most recent studies primarily concentrate on developing efficient and stretchable photoactive layers, while the stretchability of all layers in IS-OSCs and the cohesion/adhesion energies at different interfaces within these layers are essential for determining the IS-OSCs' overall mechanical properties.[1,22,28–32] Specifically, the stretchable transparent electrode (STE) is one of the key layers in determining the PCE and stretchability of the IS-OSCs, but it has been rarely studied compared to other composing layers such as active layers and top electrodes.[33–36]

To design efficient STE for IS-OSCs, the following requirements should be satisfied; (1) high transparency for allowing high light harvesting in the OSC active layer, (2) high electrical properties for the collection of charges from the active layer of OSC, and (3) excellent mechanical properties.[37–40] Considering the above requirements, poly(3,4-ethylenedioxythiophene):poly(stenesulfonate) (PEDOT:PSS) is a fascinating material as STE for its (i) excellent transmittance in ultraviolet-visible wavelength regimes[41,42] and (ii) higher mechanical robustness and ductility[43,44] compared to the inorganic-based electrodes (*i.e.* metal grids,[45] metal nanowires,[46,47] graphene,[48] and composites[49]). However, the conductivity of PEDOT:PSS is inferior to inorganic counterparts (*i.e.*, indium tin oxide (ITO)), mainly because of the electrically inactive PSS components required for the solution processability.[44,50] To address this issue, researchers have employed strong acids (*i.e.*, $H_2SO_4$, $CF_3SO_3H$, and $HNO_3$) to selectively remove the non-conductive PSS components, and have successfully increased the electrical properties of the PEDOT:PSS layer. For example, Mengistie *et al.* demonstrated $\sim 10^4$ times increase in the conductivity of PEDOT:PSS film from 0.3 to 2050 S $cm^{-1}$ by using formic acids.[51] In addition, Meng *et al.* achieved high PEDOT:PSS conductivity of 1460 S $cm^{-1}$ *via* phosphoric acid treatment, and demonstrated successful operation of flexible OSCs with the acid-treated PEDOT:PSS STE.[52]

Incorporation of acid-treated PEDOT:PSS layer with other layers has been a challenging task because the strong acids easily damage stretchable substrates including thermoplastic urethane (TPU) and poly(dimethylsiloxane) (PDMS) substrates.[43,53–55] Therefore, the direct acid treatment of the PEDOT:PSS on the substrates should be avoided. Alternatively, the PEDOT:PSS layer can be treated with the acids on the sacrificial substrate and then transferred onto the desired substrate by using various transfer methods such as stamp transfer (ST) and transfer lamination techniques. For example, Fan *et al.* transferred the acid-treated PEDOT:PSS onto the PDMS substrate by ST-method and demonstrated very high conductivity of the transferred PEDOT:PSS STE.[55] However, the interfaces between the physically transferred PEDOT:PSS and stretchable substrate are often not conformal, which results in weak adhesion and low mechanical integrity between the two layers. This weak adhesion with bonding energy <1 kJ $mol^{-1}$ at the substrate-PEDOT:PSS interfaces often cause stripping and delamination of the PEDOT:PSS layer during the stretching, limiting the stretchability of the IS-OSC devices.[56,57]

Forming an interdiffused zone between the adjacent layers is an effective approach to promoting adhesion strength between the two layers. Because the interfaces between the two layers can be enlarged by the interdiffusion of each constituting material, the conformal contact between the layers can be achieved over the large area, and thus the adhesion strength between the layers can be significantly strengthened compared to that obtained by the conventional physical transfer methods.[58,59] For example, Daelemans *et al.* reported a significant increase in the adhesion energy ($G$) of poly(ε-caprolactone):epoxy interfaces from 400 to 650 J $m^{-2}$ by promoting interdiffusion between the layers.[60] Therefore, the construction of the molecular interdiffused zone between the stretchable substrate and PEDOT:PSS layer will strengthen the adhesion properties between the two layers, and contribute to the mechanical robustness and stretchability of the IS-OSCs.

In this study, we demonstrate highly efficient (PCE = 13.1%) and mechanically robust (strain at $PCE_{80\%} = 34\%$) IS-OSCs by developing a molecular interdiffusion (MID)-assisted TPU-PEDOT:PSS bilayer. We observe that the interdiffusion between PEDOT:PSS and TPU molecules significantly strengthens adhesion at their interfaces, affording 3-times higher adhesion energy of the MID-assisted TPU-PEDOT:PSS (45.0 J $m^{-2}$) compared to the conventional ST-based TPU-PEDOT:PSS (15.1 J $m^{-2}$). Using a finite element model (FEM) simulation, we demonstrate that the MID-based bilayer more effectively dissipates mechanical stress than the ST-based bilayer due to its stronger adhesion, which significantly improves the stretchability of the bilayer by preventing interfacial crackings. As a result, the IS-OSCs featuring MID-based TPU-PEDOT:PSS bilayer achieve excellent stretchability (strain at $PCE_{80\%} = 34\%$), which outperforms that of the conventional ST-based devices (strain at $PCE_{80\%} = 17\%$). In addition, we demonstrate the general applicability of the MID-assisted STE/substrate bilayer for achieving other high-performance IS-OSCs with various active materials.

## 2. Results and discussion

### 2.1 Development of STEs and their properties

The important requirements for the PEDOT:PSS-based STEs are high optical transmittance, electrical properties, and mechanical robustness.[42,43,61] To improve the conductivity of PEDOT:PSS layer, we used perchloric acid ($HClO_4$) to selectively remove the electrically inactive PSS components in PEDOT:PSS. Detailed procedures for the $HClO_4$ treatment are provided in ESI.† The $HClO_4$-treated PEDOT:PSS exhibited a 1.5-fold higher conductivity of 961 S $cm^{-1}$ than the neat PEDOT:PSS (conductivity = 605 S $cm^{-1}$).[62] In addition, the $HClO_4$-treated PEDOT:PSS film showed higher transmittances in a wide wavelength range of 400–1000 nm compared to the pristine PEDOT:PSS film owing to the removal of PSS contents in films (Fig. S1 and Table S1†).[63] More distinct PEDOT fibrillar features of the $HClO_4$-treated PEDOT:PSS surfaces than the neat PEDOT:PSS film in atomic force microscopy (AFM) images indicate the removal of PSS

components in $HClO_4$-treated PEDOT:PSS film (Fig. S2†).[64] As a result, the acid-treated PEDOT:PSS used in this study demonstrates an excellent figure of merit (FoM) regarding transmittance and conductivity of 84, which is significantly higher than the typical industrial requirement of STEs (FoM ~35).[42,53,65]

We employed thermoplastic urethane (TPU) as stretchable substrates to construct IS-OSCs, since it has relatively high optical transmittance and low surface roughness among the elastomers.[10–12,14,61] Conventionally, the acid-treated PEDOT:PSS layers have been transferred by physical transfer methods (*i.e.*, stamp transfer),[41,54] but the adhesion properties at the interfaces of the physically transferred PEDOT:PSS and TPU are typically poor due to the non-conformal contact (Fig. 1a). These weak adhesion properties can limit the overall stretchability of IS-OSCs. To reinforce the adhesion between the PEDOT:PSS layer and TPU substrate, we developed a MID-assisted TPU-PEDOT:PSS bilayer by spin-casting of the TPU solution onto the $HClO_4$-treated PEDOT:PSS film. We aimed to diffuse TPU molecules into the PEDOT network and form an interdiffused zone with the large and conformal interfaces, which, in turn, enhances the adhesion properties and mechanical robustness of the TPU-PEDOT:PSS bilayer (Fig. 1b). To demonstrate the effectiveness of the MID-assisted TPU-PEDOT:PSS bilayer, we also construct the reference TPU-PEDOT:PSS bilayer systems using standard stamp transfer (ST) method.[40,59] The detailed fabrication procedures and conditions for ST- and MID-based TPU-PEDOT:PSS bilayers are provided in Experimental section and Fig. S3.† Both ST- and MID-based TPU-PEDOT:PSS exhibited comparably high UV-vis transmittance ($T = 95\%$ at 550 nm) and low sheet resistance ($R_{sh}$) values (80–90 Ω $sq^{-1}$), rendering them suitable for high-performance STEs (Fig. S4† and Table 1).[42,44] We note that the transmittance of the TPU-PEDOT:PSS was higher than ITO-based electrode (Table 1), which is beneficial for increasing light-harvesting in the photoactive layer and achieving a high short-circuit current density ($J_{sc}$) value of IS-OSCs. While both the optical transmittance and electrical properties (conductivity and work function, Table S1 and Fig. S5†) of the ST- and MID-based TPU-PEDOT:PSS are comparable, we observed that the surface of MID-based TPU-PEDOT:PSS bilayer was more homogeneous and uniform than that of the ST-based TPU-PEDOT:PSS (Fig. S6†).

We then investigated the adhesion properties of the ST- and MID-based TPU-PEDOT:PSS bilayers (Fig. 2a and b). We measured cohesive energy ($G_c$) of TPU-PEDOT:PSS by performing a double cantilever beam (DCB) test (Fig. S7† and Table 1).[66] The $G_c$ of MID-based TPU-PEDOT:PSS (45.0 J $m^{-2}$) was 3-times higher than ST-based TPU-PEDOT:PSS ($G_c$ = 15.1 J $m^{-2}$)

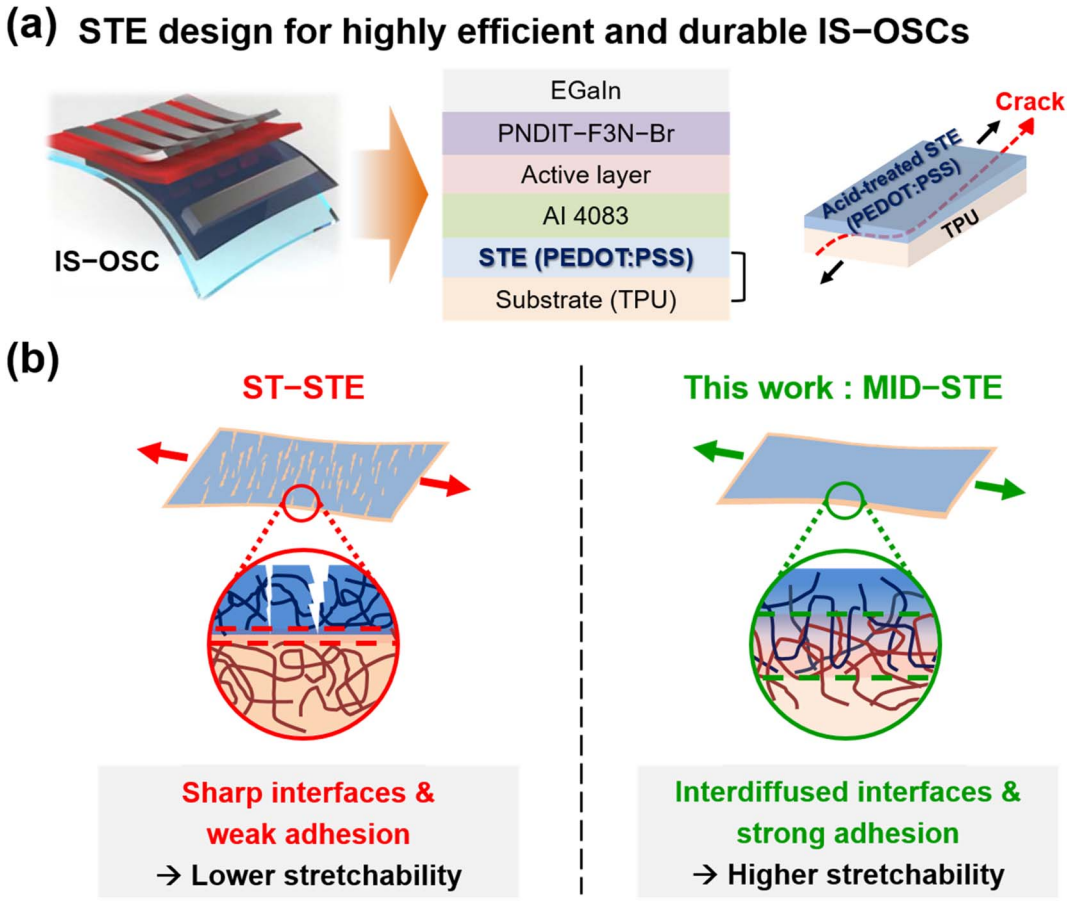


Fig. 1 (a) Device structure of the IS-OSC and (b) schematics describing different interfacial and adhesion properties of ST- and MID-assisted stretchable transparent electrodes (STEs).

 

Table 1 Optoelectrical properties, fracture energy and peel strength of ITO, ST- and MID-based TPU-PEDOT:PSS bilayers

| Substrate | $T_{550nm}$[a] (%) | $R_{sh}$[b] (Ω sq$^{-1}$) | FoM[c] | $G_c$[d] (J m$^{-2}$) | Peel strength[e] (N m$^{-1}$) |
|---|---|---|---|---|---|
| ITO | 91.0 | 8 ± 1 | 488 | — | — |
| TPU/PEDOT:PSS (ST) | 95.2 | 90 ± 5 | 84 | 15.1 | 7.7 |
| TPU/PEDOT:PSS (MID) | 95.1 | 88 ± 2 | 84 | 45.0 | 50.6 |

[a] Transmittance at 550 nm. [b] Average values obtained from more than five samples. [c] The ratio of direct current conductivity ($\sigma_{dc}$) to optical conductivity ($\sigma_{op}$). FoM $= \frac{\sigma_{dc}}{\sigma_{op}} = \frac{Z_0}{2R_{sheet}\left(T^{-\frac{1}{2}} - 1\right)}$; $T$ = transmittance (%, at $\lambda$ = 550 nm), $Z_0$ = (impedance of free space, 377 Ω). [d] Measured by DCB test. [e] Measured by 90° peel test.

(Fig. 2b). The 90° peel test further confirm the significant difference in the adhesion properties between the MID-based and ST-based TPU-PEDOT:PSS (Fig. S8 and S9†).[67] Notably, the peel strength of the MID system (50.6 ± 5.9 N m$^{-1}$) was 6.5-fold higher than the ST system (peel strength = 7.7 ± 2.1 N m$^{-1}$) (Fig. S9† and Table 1). The higher peel strength and $G_c$ of the MID-based TPU-PEDOT:PSS demonstrate the stronger adhesion between PEDOT:PSS and TPU layers compared to that in the ST-based TPU-PEDOT:PSS.

To visualize the contrast in the adhesion properties between the ST-based and MID-based TPU-PEDOT:PSS bilayers, we sonicated the two different TPU-PEDOT:PSS bilayers in water for 20 min (Fig. 2c). We observed that the PEDOT:PSS layer in the MID-based TPU-PEDOT:PSS was well maintained without any delamination, whereas the PEDOT:PSS film in ST-based TPU-PEDOT:PSS was exfoliated after the sonification (Fig. 2c). The origin of the significantly higher adhesion properties of MID-based TPU-PEDOT:PSS was further investigated by the depth profiles of the two different TPU-PEDOT:PSS systems using a time-of-flight secondary ion mass spectrometry (ToF-SIMS).[68,69] During the ion sputtering, the relative compositions of the TPU and PEDOT:PSS layers were tracked by their main

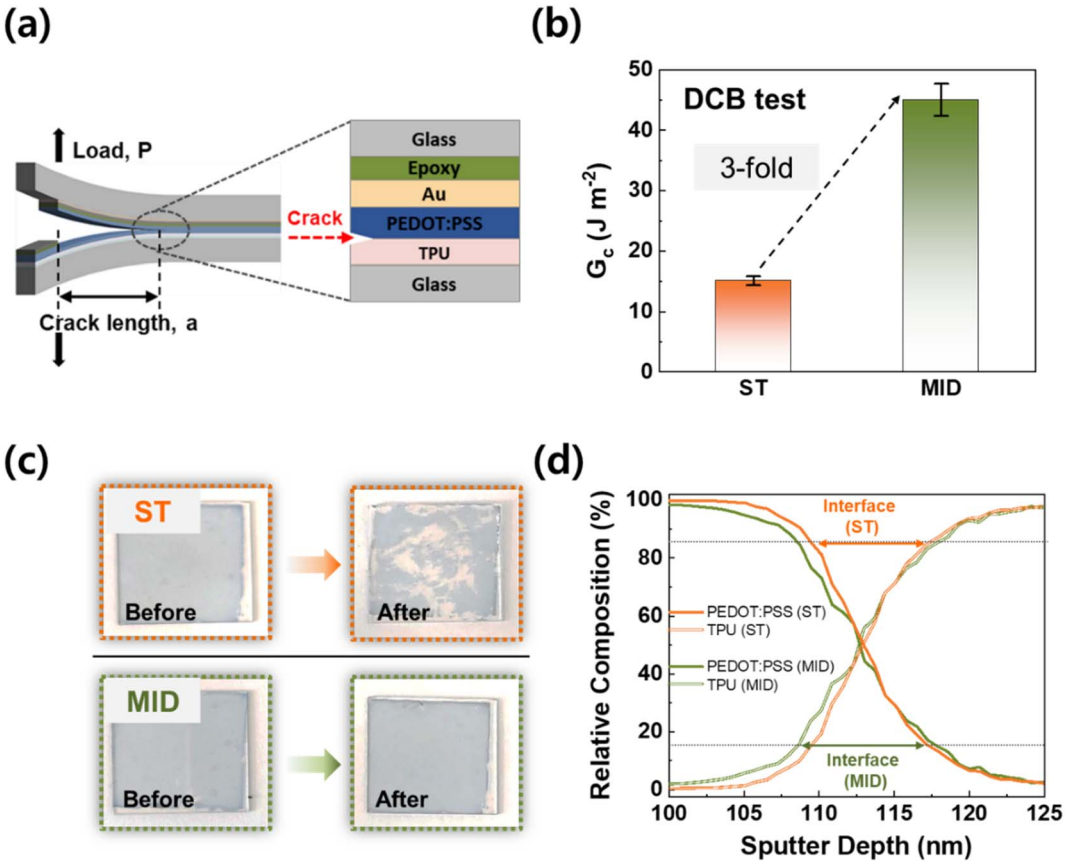


Fig. 2 (a) Schematic description of the DCB (double cantilever beam) test. (b) $G_c$s measured by DCB test, (c) optical images of adhesion test samples (20 min of sonication in water) with ST- and MID-based TPU-PEDOT:PSS bilayers, and (d) ToF-SIMS (time-of-flight secondary ion mass spectrometry) depth profiles of ST- and MID-based TPU-PEDOT:PSS bilayers.

components of $OCN^-$ and $C_8H_7SO_3^-$, respectively (Fig. 2d). The MID-based TPU-PEDOT:PSS exhibited a broader interfacial width compared to that of the ST-based TPU-PEDOT:PSS (Fig. 2d), which supports the interdiffusion of the TPU and PEDOT:PSS domains near at the interface.[69,70]

### 2.2 IS-OSC performances

Next, we compared photovoltaic and mechanical properties of IS-OSCs using the ST- and MID-based TPU:PEDOT:PSS bilayers. Device structures and fabrication procedures of IS-OSCs followed our previous literature,[71] which are detailed in Experimental section of the ESI.† We fabricated IS-OSCs with four different active layer systems of (1) PM6:Y6,[72,73] (2) PM6-OEG5:BTP-eC9,[12] (3) PBDB-T:PYBDT-Cl,[30] and (4) PM6:Y6-BO:N2200 (ref. 8) to demonstrate effectiveness of the MID-based TPU-PEDOT:PSS. These systems represent the efficient photoactive systems of (1–2) polymer donor:small molecule acceptor, (3) all-polymer donor and acceptor, and (4) ternary blends. The chemical structures of the active materials are

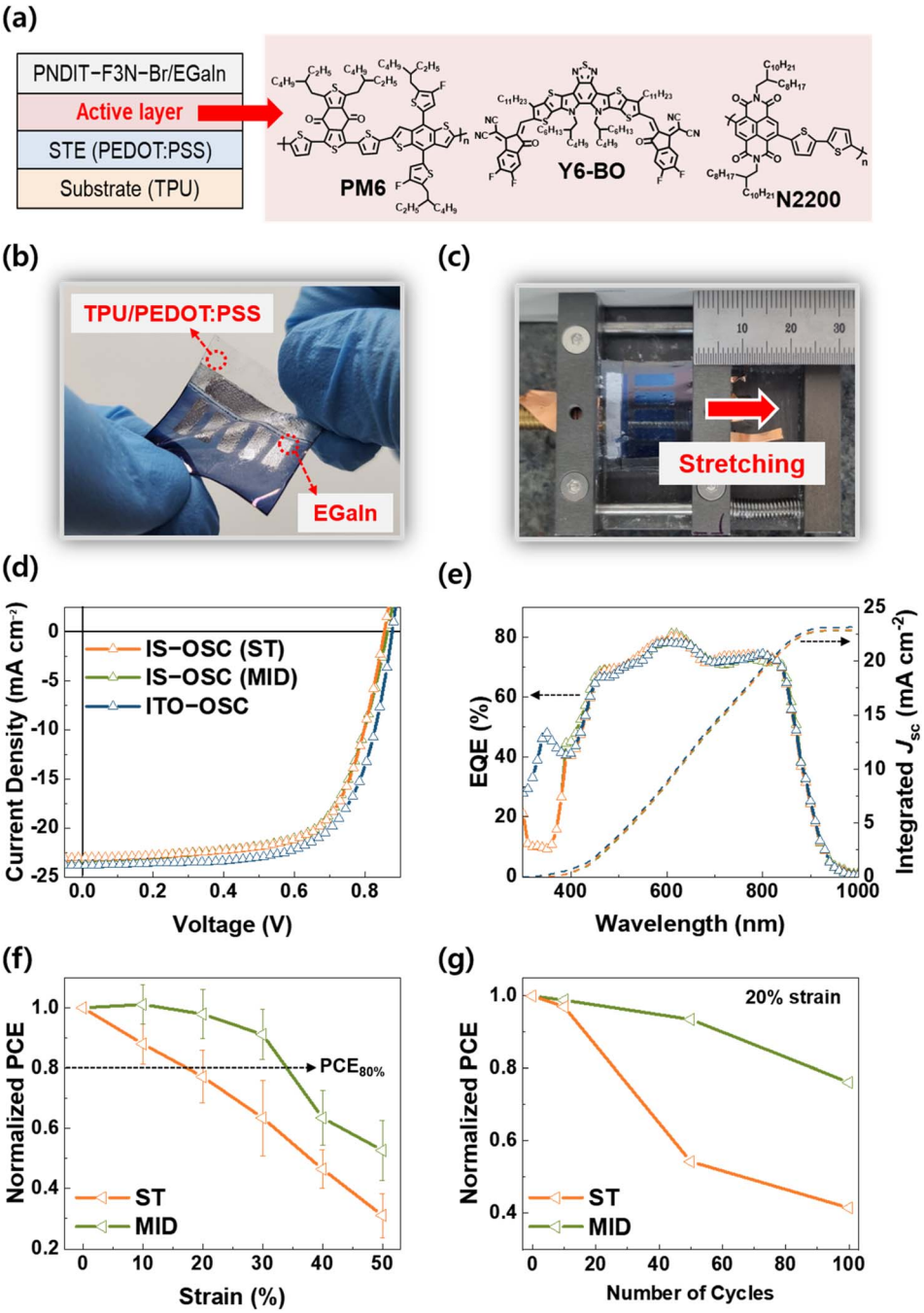


Fig. 3 (a) Chemical structures of PM6, Y6-BO, and N2200; (b) device structure and (c) experimental setup for the stretching test of IS-OSCs; (d) *J–V* curves and (e) EQE spectra of PM6:Y6-BO:N2200 based IS-OSCs; (f) normalized PCE of IS-OSCs under strains; (g) normalized PCE as a function of the number of stretching cycles at 20% strain.

 

Table 2 Photovoltaic characteristics of PM6:Y6-BO:N2200 OSCs based on different bottom electrodes

| Substrate | $V_{oc}$ (V) | $J_{sc}$ (mA cm$^{-2}$) | Cal. $J_{sc}$[a] (mA cm$^{-2}$) | FF (%) | $PCE_{max}$ ($PCE_{avg}$)[b] (%) |
|---|---|---|---|---|---|
| ITO | 0.88 (0.87 ± 0.00) | 23.8 (23.7 ± 0.2) | 23.1 | 67.5 (67.8 ± 0.4) | 14.1 (14.0 ± 0.1) |
| TPU/PEDOT:PSS (ST) | 0.85 (0.85 ± 0.00) | 23.0 (23.2 ± 0.3) | 22.8 | 67.8 (64.6 ± 2.2) | 13.3 (12.8 ± 0.4) |
| TPU/PEDOT:PSS (MID) | 0.85 (0.85 ± 0.00) | 23.2 (22.8 ± 0.6) | 22.9 | 65.9 (66.3 ± 1.2) | 13.1 (12.9 ± 0.2) |

[a] Calculated from integration of the EQE spectra. [b] The parameters represent average values measured from more than five devices.

shown in Fig. S10.† Among these active layer systems, we mainly employed the PM6:Y6-BO:N2200 active layer system in the IS-OSCs for comparing the ST-based and MID-based TPU-PEDOT:PSS bilayers (Fig. 3a), because the previous study reported that the PM6:Y6-BO:N2200-based IS-OSC devices showed high PCE and mechanical stretchability (Tables S3 and S4†).[11]

Device images and measuring setups for the IS-OSCs are displayed in Fig. 3b and c, respectively. Current density–voltage (*J–V*) and external quantum efficiency (EQE) curves of the PM6:Y6-BO:N2200-based devices are shown in Fig. 3d and e, respectively. The photovoltaic parameters are provided in Table 2. We observed that the IS-OSCs exhibited greater variations in photovoltaic parameters compared to ITO-devices, due to the use of PEDOT and liquid metal-based electrodes. The PM6:Y6-BO:N2200-based IS-OSCs using ST- and MID-based TPU-PEDOT:PSS exhibited similarly high PCEs of 13.1–13.3% (Table 2). The IS-OSC PCEs correspond to 93–94% of ITO-OSC PCEs (14.1%), which are significantly higher than those of the reported IS-OSCs.[8,12–14,20] The high photovoltaic performances of the IS-OSCs comparable to the ITO-OSCs in this work are mainly attributed to the excellent transmittance and conductivity of the $HClO_4$-treated PEDOT:PSS layer. Calculated $J_{sc}$s from external quantum efficiency (EQE) spectra of IS-OSCs were well matched with device $J_{sc}$s (Fig. 3e).

Next, we investigated the mechanical stability of two different IS-OSCs with ST- and MID-based TPU-PEDOT:PSS layers by tracking their PCEs during the stretching. The test was performed for more than 3 times for each device system and the average PCE values with standard deviations were used in Fig. 3f. The representative data are shown in Tables S3–S10 and Fig. S11.† The normalized PCE plots of these IS-OSCs as a function of strain show that the stretchability of the MID-based TPU-PEDOT:PSS was significantly higher than that of ST-based TPU-PEDOT:PSS. For example, the MID-based IS-OSCs retained 80% of the initial PCE even at a 34% strain (strain at $PCE_{80\%}$ = 34%), whereas the PCE of the ST-based device decreased to 56% of its initial PCE value at the same strain of 34%. The strain at $PCE_{80\%}$ for the ST-based IS-OSCs was only 17%. We note that the PM6:Y6-BO:N2200-based IS-OSCs featuring MID-based TPU-PEDOT:PSS achieved the highest PCE and stretchability among the reported IS-OSCs (Fig. S12 and Table S11†). To demonstrate the general applicability of the MID-based TPU-PEDOT:PSS film, we compared the ST-based and MID-based IS-OSCs using different active layer systems including PM6:Y6, PM6-OEG5:BTP-eC9, and PBDB-T:PYBDT-Cl materials (Fig. S11 and Tables S5–S10†). Regardless of the active layer system, the MID-based IS-OSCs exhibited significantly superior stretchability performances compared to those of the ST-based IS-OSCs. We also monitored the PCEs under repetitive stretching/releasing with a fixed strain of 20% to assess the durability of the IS-OSCs (Fig. 3g). In the cyclic tests under repetitive stretching/releasing, the MID-based IS-OSC maintained over 80% of the initial PCE after 100-times stretching with a fixed strain of 20%. However, the ST-based devices showed only 42% of the initial PCE after the same stretching cycles.

### 2.3 Mechanical properties of STEs

To further elucidate the origin of excellent device stretchability of MID-based IS-OSCs, we investigated the mechanical properties of MID- and ST-based TPU-PEDOT:PSS bilayers (Fig. 4). The resistances of each TPU-PEDOT:PSS were monitored as a function of engineering strain and stretching cycles at 20% strain. The ST-based TPU-PEDOT:PSS experienced rapid increases of relative resistance (resistance ($R$)/initial resistance ($R_0$)) up to 4.0 at 50% strain, indicating a considerable decrease of electrical properties under the strain (Fig. 4a). In contrast, the MID-based TPU-PEDOT:PSS retained superior electrical properties with $R/R_0 \sim 2.5$ at the same 50% strain. A similar trend was observed in the cyclic tests. For instance, the $R/R_0$ of ST-based TPU-PEDOT:PSS rapidly increased to 3.0 after 500-times of stretching cycles with 20% strain, whereas the MID-based TPU-PEDOT:PSS maintained a smaller $R/R_0$ of 1.7 after the same cycling conditions (Fig. 4b). The origin of the superior mechanical robustness and stretchability of the ST-based TPU-PEDOT:PSS can be supported by the film morphology of the TPU-PEDOT:PSS under various strains (Fig. 4c). The ST-based TPU-PEDOT:PSS showed cracks after 10% strained, and the cracks became larger and sharper with increasing strain. In contrast, the MID-based TPU-PEDOT:PSS showed no crack until 30% strain. The higher stretchability of MID-based TPU-PEDOT:PSS compared with ST-based TPU-PEDOT:PSS is consistent with the superior device durability of corresponding IS-OSCs.

### 2.4 Finite element simulation

To better understand the relationship between the adhesion properties of TPU-PEDOT:PSS STE and the overall stretchability of the IS-OSC device, we performed a finite element method (FEM) simulation (Fig. 5).[74,75] This simulation model can describe the interfacial crack propagation between the bilayers using a virtual crack closure technique (VCCT) and the resultant planar crack driving forces within the PEDOT:PSS STE layer using *J*-integral analysis. Based on the reported material

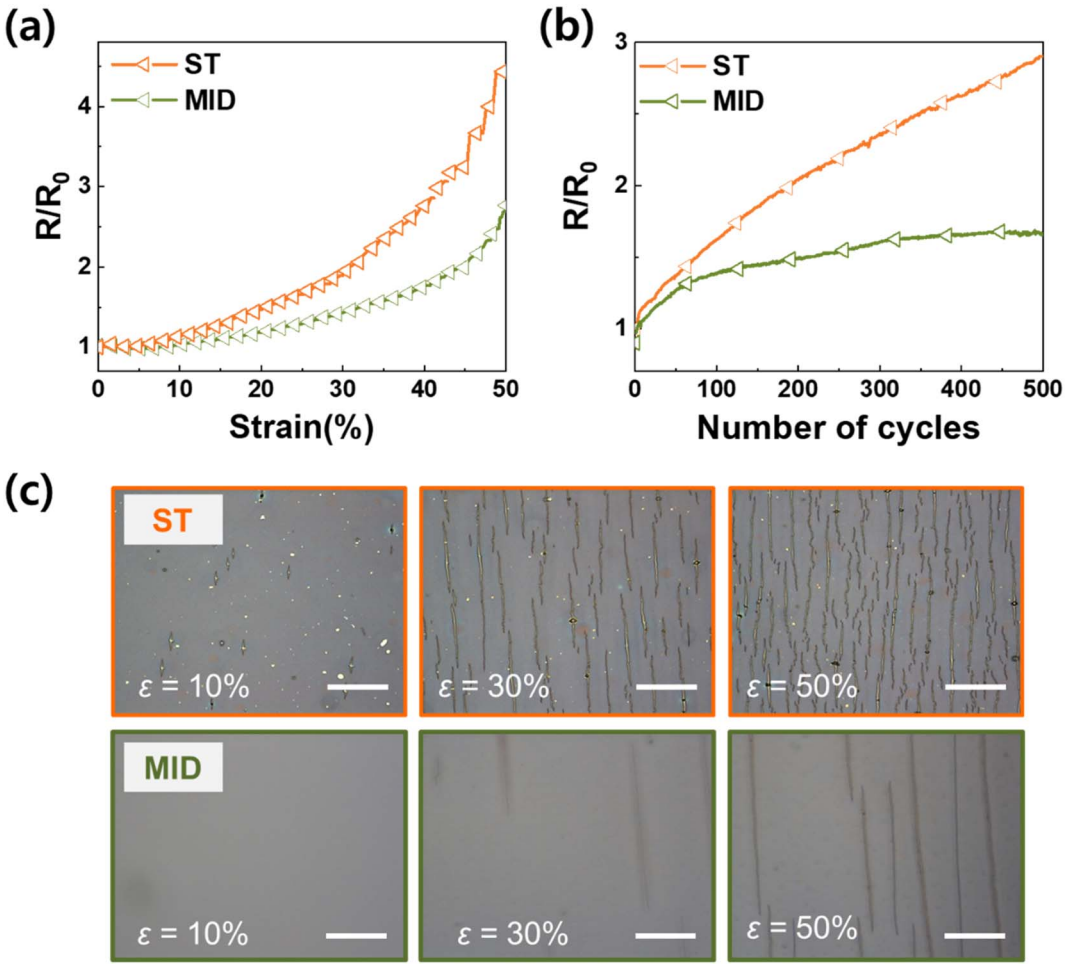


Fig. 4 (a) Resistance variation as a function of tensile strain up to 50% strain of MID- and ST-based TPU-PEDOT:PSS; (b) relative resistance *versus* number of cycles (20% strain cycle condition) of MID- and ST-based TPU-PEDOT:PSS; (c) optical microscopy images of MID- and ST-based TPU-PEDOT:PSS at 10%, 30% and 50% stretched positions, scale bar = 100 μm.

properties of PEDOT:PSS and TPU, we assumed the cuboid-shaped TPU-PEDOT:PSS bilayers for simulation.[43,76,77] The detailed simulation procedures and boundary conditions are described in Experimental section of the ESI.† We characterized the mechanical properties with the planar crack driving force ($J_{planar}$) as a function of strain at different critical interfacial energy release rates ($G_{c,int}$).[78] The $J_{planar}$ indicates the driving forces for in-plane cracking of the top PEDOT:PSS layer, and the in-plane cracking occurs when the $J_{planar}$ values reach to the critical crack driving forces ($J_c$s) of the top layer. As the value of $G_{c,int}$ represents the adhesion force between TPU and PEDOT:PSS layers, we varied $G_{c,int}$ from 1 to 5 J m$^{-2}$ to simulate the bilayers with different adhesion strengths. We used smaller $G_{c,int}$ values (1−5 J m$^{-2}$) than the measured $G_c$s from the DCB test (15.1–45.0 J m$^{-2}$) to simplify the simulation. Then, we estimated $J_{planar}$, which represents driving force for the in-plane cracking within a PEDOT:PSS layer under strain depending on the $G_{c,int}$.[78]

The increased $J_{planar}$ within the PEDOT:PSS layer with increasing strain indicates the accelerated in-plane crackings upon increasing the strain of PEDOT:PSS and TPU layers (Fig. 5a). Notably, we observed that the $J_{planar}$ values were effectively decreased with increasing $G_{c,int}$ of TPU-PEDOT:PSS. For example, the $J_{planar}$ at 12% strain of TPU-PEDOT:PSS decreased from 98.8 to 68.1 J m$^{-2}$ as the $G_{c,int}$ increased from 1 to 5 J m$^{-2}$ (Fig. 5b). In interfacial bonding state and stress distribution images, the TPU-PEDOT:PSS with low adhesion energy (1 J m$^{-2}$, representing ST-based TPU-PEDOT:PSS) showed larger interfacial delamination and less stressed TPU layer when 10% strained (Fig. 5c). In contrast, the TPU-PEDOT:PSS with 3-times higher adhesion energy (3 J m$^{-2}$, representing MID-based TPU-PEDOT:PSS) exhibited smaller interfacial delamination and more stressed TPU layer under the same strain (Fig. 5d). These results demonstrate that the higher adhesion energy between TPU and PEDOT:PSS effectively decreases delamination at their interfaces and dissipates mechanical stress to TPU layer, which consequently reduces the driving forces for in-plane cracking at the PEDOT:PSS layer. Therefore, the simulation results well explain the superior stretchability and durability of MID-based IS-OSCs to those of ST-based IS-OSCs.

 

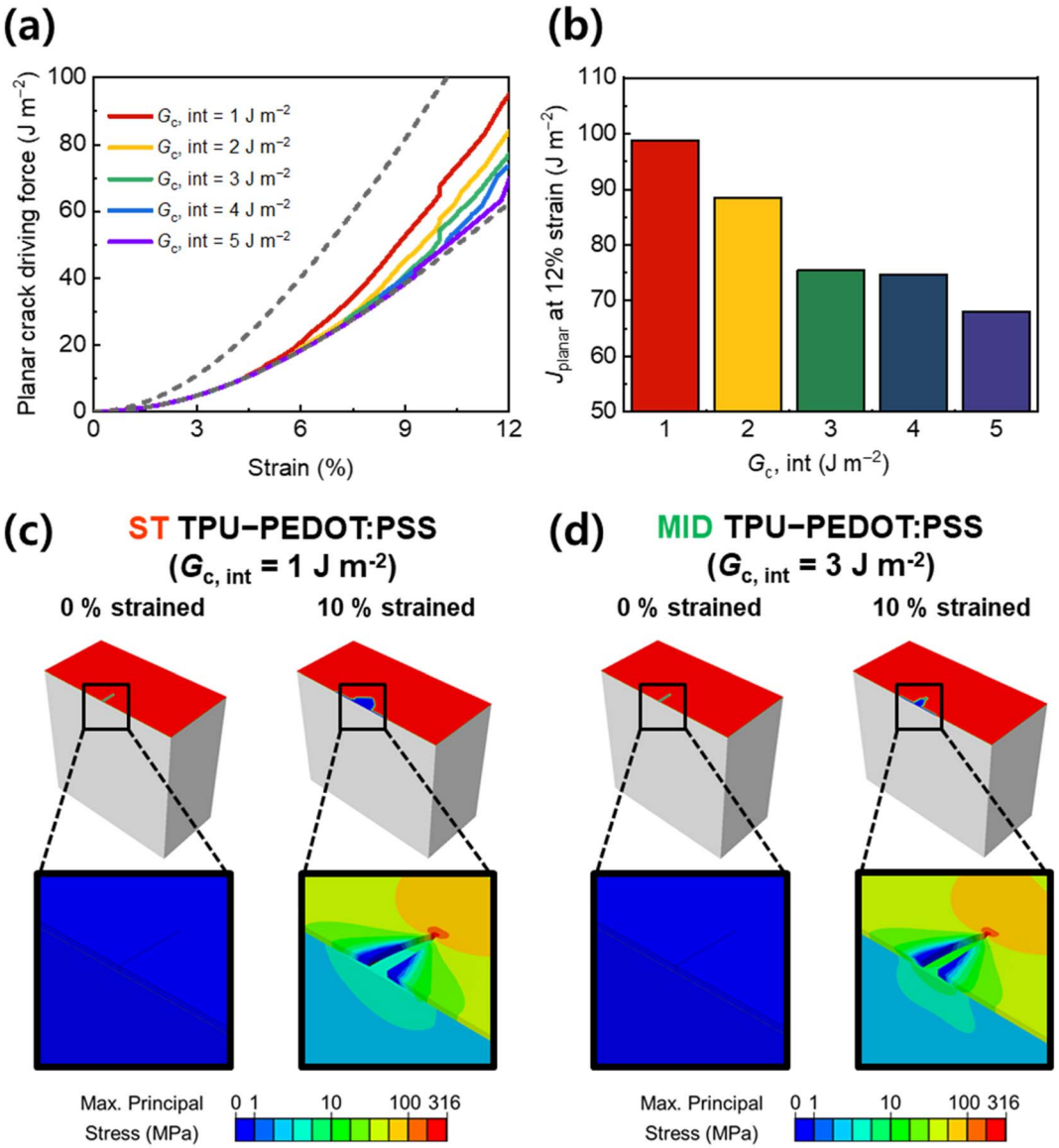


Fig. 5 (a) Planar crack driving force ($J_{planar}$) as a function of strain (gray dotted lines represent $J_{planar}$ at boundary conditions; upper line = no adhesion, lower line = perfect adhesion) and (b) $J_{planar}$ at 12% strain depending on the initial $G_c$s of the bilayers. (c and d) Interfacial boding state and stress distribution images before and after 10% strained of the bilayers having $G_c$ values of (c) 1 and (d) 3 J m$^{-2}$, respectively; the former and latter models represent ST- and MID-based bilayers, respectively.

## 3. Conclusions

We achieved efficient (PCE = 13.1%) and highly stretchable (strain at $PCE_{80\%}$ = 34%) IS-OSCs by developing a MID-based TPU-PEDOT:PSS interdiffused bilayer with a strong adhesion force at the interface. The MID-assisted TPU-PEDOT:PSS exhibited excellent transparency and conductivity, which led to the high performance of the resulting IS-OSCs with a PCE of 13.1%. Importantly, the MID-based TPU-PEDOT:PSS exhibited significantly higher adhesion energy ($G_c$ = 45.0 J m$^{-2}$) between TPU and PEDOT:PSS layers compared to the ST-based TPU-PEDOT:PSS ($G_c$ = 15.1 J m$^{-2}$). Also, the MID-based IS-OSCs showed significantly higher stretchability (strain at $PCE_{80\%}$ = 34%) compared to the ST-based IS-OSCs (strain at $PCE_{80\%}$ = 17%). While we successfully demonstrated that the MID-based TPU-PEDOT:PSS bilayer can significantly enhance the stretchability of different IS-OSCs with various photoactive materials, the PM6:Y6-BO:N2200-based IS-OSCs featuring MID-based TPU-PEDOT:PSS achieved the highest PCE and stretchability among the reported IS-OSCs. Combined experimental and simulation analyses on the mechanical properties of the ST- and MID-based TPU-PEDOT:PSS bilayers reveal that improved $G_c$ value of the MID-based TPU-PEDOT:PSS contributed to the increase of the tensile properties of the bilayer as well as the device stretchability of corresponding IS-OSCs. Therefore, this study demonstrates the importance of adhesion interactions between the constituent layers in the OSCs for constructing IS-OSCs with high mechanical stretchability and reliability.

## Conflicts of interest

There are no conflicts to declare.

## Acknowledgements

This research was supported by the National Research Foundation of Korea (2017M3A7B8065584, 2020M3H4A1A02084906, and 2017M3D1A1039553). This research is additionally performed as a cooperation project of "Basic project", supported by the Korea Research Institute of Chemical Technology (KRICT).

## References

1 W. C. Huang, Z. Jiang, K. Fukuda, X. C. Jiao, C. R. McNeill, T. Yokota and T. Someya, *Joule*, 2020, **4**, 128–141.
2 S. A. Hashemi, S. Ramakrishna and A. G. Aberle, *Energy Environ. Sci.*, 2020, **13**, 685–743.
3 T. Q. Trung and N. E. Lee, *Adv. Mater.*, 2017, **29**, 1603167.
4 V. Vallem, Y. Sargolzaeiaval, M. Ozturk, Y.-C. Lai and M. D. Dickey, *Adv. Mater.*, 2021, **33**, 2004832.
5 J.-W. Lee, C. Sun, S. W. Lee, G. U. Kim, S. Li, C. Wang, T. S. Kim, Y. H. Kim and B. J. Kim, *Energy Environ. Sci.*, 2022, **15**, 4672–4685.
6 J. Qin, L. Lan, S. Chen, F. Huang, H. Shi, W. Chen, H. Xia, K. Sun and C. Yang, *Adv. Funct. Mater.*, 2020, **30**, 2002529.
7 P. B. J. St. Onge, M. U. Ocheje, M. Selivanova and S. Rondeau-Gagné, *Chem. Rec.*, 2019, **19**, 1008–1027.
8 J.-W. Lee, G. U. Kim, D. J. Kim, Y. Jeon, S. Li, T. S. Kim, J. Y. Lee and B. J. Kim, *Adv. Energy Mater.*, 2022, **12**, 2200887.
9 C. Yan and P. S. Lee, *Small*, 2014, **10**, 3443–3460.
10 K. Xie and B. Wei, *Adv. Mater.*, 2014, **26**, 3592–3617.
11 J. B. H. Tok and Z. Bao, *Sci. China Chem.*, 2012, **55**, 718–725.
12 J.-W. Lee, C. Lim, S. W. Lee, Y. Jeon, S. Lee, T. S. Kim, J. Y. Lee and B. J. Kim, *Adv. Energy Mater.*, 2022, **12**, 2202224.
13 Z. Y. Wang, D. Zhang, M. C. Xu, J. F. Liu, J. Y. He, L. Yang, Z. L. Li, Y. R. Gao and M. Shao, *Small*, 2022, **18**, 2201589.
14 J.-W. Lee, S. Seo, S.-W. Lee, G.-U. Kim, S. Han, T. N.-L. Phan, S. Lee, S. Li, T.-S. Kim, J.-Y. Lee and B. J. Kim, *Adv. Mater.*, 2022, **34**, 2207544.
15 S. Savagatrup, A. S. Makaram, D. J. Burke and D. J. Lipomi, *Adv. Funct. Mater.*, 2014, **24**, 1169–1181.
16 Y. T. Hsieh, J. Y. Chen, S. Fukuta, P. C. Lin, T. Higashihara, C. C. Chueh and W. C. Chen, *ACS Appl. Mater. Interfaces*, 2018, **10**, 21712–21720.
17 D. J. Lipomi, B. C. K. Tee, M. Vosgueritchian and Z. Bao, *Adv. Mater.*, 2011, **23**, 1771–1775.
18 M. Amjadi, Y. J. Yoon and I. Park, *Nanotechnology*, 2015, **26**, 375501.
19 Y. Hu, J. Wang, C. Yan and P. Cheng, *Nat. Rev. Mater.*, 2022, **7**, 836–838.
20 Z. Wang, M. Xu, Z. Li, Y. Gao, L. Yang, D. Zhang and M. Shao, *Adv. Funct. Mater.*, 2021, **31**, 2103534.
21 C. Yan, J. Qin, Y. Wang, G. Li and P. Cheng, *Adv. Energy Mater.*, 2022, **12**, 2201087.
22 Q. P. Fan, W. Y. Su, S. S. Chen, W. Kim, X. B. Chen, B. Lee, T. Liu, U. A. Mendez-Romero, R. J. Ma, T. Yang, W. L. Zhuang, Y. Li, Y. W. Li, T. S. Kim, L. T. Hou, C. Yang, H. Yan, D. H. Yu and E. G. Wang, *Joule*, 2020, **4**, 658–672.
23 S. S. Chen, S. Jung, H. J. Cho, N. H. Kim, S. Jung, J. Q. Xu, J. Oh, Y. Cho, H. Kim, B. Lee, Y. An, C. F. Zhang, M. Xiao, H. Ki, Z. G. Zhang, J. Y. Kim, Y. F. Li, H. Park and C. Yang, *Angew. Chem., Int. Ed.*, 2018, **57**, 13277–13282.
24 C. Y. Chang, Y. J. Cheng, S. H. Hung, J. S. Wu, W. S. Kao, C. H. Lee and C. S. Hsu, *Adv. Mater.*, 2012, **24**, 549–553.
25 O. Awartani, B. I. Lemanski, H. W. Ro, L. J. Richter, D. M. DeLongchamp and B. T. O'Connor, *Adv. Energy Mater.*, 2013, **3**, 399–406.
26 N. Balar, J. J. Rech, R. Henry, L. Ye, H. Ade, W. You and B. T. O'Connor, *Chem. Mater.*, 2019, **31**, 5124–5132.
27 S. Savagatrup, A. D. Printz, T. F. O'Connor, A. V. Zaretski, D. Rodriquez, E. J. Sawyer, K. M. Rajan, R. I. Acosta, S. E. Root and D. J. Lipomi, *Energy Environ. Sci.*, 2015, **8**, 55–80.
28 H. L. Sun, B. Liu, Y. L. Ma, J.-W. Lee, J. Yang, J. W. Wang, Y. C. Li, B. B. Li, K. Feng, Y. Q. Shi, B. H. Zhang, D. X. Han, H. Meng, L. Niu, B. J. Kim, Q. D. Zheng and X. G. Guo, *Adv. Mater.*, 2021, **33**, 2102635.
29 B. Liu, H. L. Sun, J.-W. Lee, J. Yang, J. W. Wang, Y. C. Li, B. B. Li, M. Xu, Q. G. Liao, W. Zhang, D. X. Han, L. Niu, H. Meng, B. J. Kim and X. G. Guo, *Energy Environ. Sci.*, 2021, **14**, 4499–4507.
30 J.-W. Lee, D. Jeong, D. J. Kim, T. N. L. Phan, J. S. Park, T. S. Kim and B. J. Kim, *Energy Environ. Sci.*, 2021, **14**, 4067–4076.
31 J.-W. Lee, S. W. Lee, J. Kim, Y. H. Ha, C. Sun, T. N. L. Phan, S. Lee, C. Wang, T. S. Kim, Y. H. Kim and B. J. Kim, *J. Mater. Chem. A*, 2022, **10**, 20312–20322.
32 Q. N. Chen, Y. H. Han, L. R. Franco, C. F. N. Marchiori, Z. Genene, C. M. Araujo, J.-W. Lee, T. N. L. Phan, J. N. Wu, D. H. Yu, D. J. Kim, T. S. Kim, L. T. Hou, B. J. Kim and E. G. Wang, *Nano-Micro Lett.*, 2022, **14**, 1–14.
33 D. J. Lipomi and Z. Bao, *Energy Environ. Sci.*, 2011, **4**, 3314–3328.
34 E. Dauzon, X. Sallenave, C. Plesse, F. Goubard, A. Amassian and T. D. Anthopoulos, *Adv. Mater.*, 2021, **33**, 2101469.
35 M. D. Dickey, R. C. Chiechi, R. J. Larsen, E. A. Weiss, D. A. Weitz and G. M. Whitesides, *Adv. Funct. Mater.*, 2008, **18**, 1097–1104.
36 R. C. Chiechi, E. A. Weiss, M. D. Dickey and G. M. Whitesides, *Angew. Chem., Int. Ed.*, 2008, **47**, 142–144.
37 K. S. Kim, Y. Zhao, H. Jang, S. Y. Lee, J. M. Kim, K. S. Kim, J. H. Ahn, P. Kim, J. Y. Choi and B. H. Hong, *Nature*, 2009, **457**, 706–710.
38 J. Zhang, X. J. Liu, W. J. Xu, W. H. Luo, M. Li, F. B. Chu, L. Xu, A. Y. Cao, J. S. Guan, S. M. Tang and X. J. Duan, *Nano Lett.*, 2018, **18**, 2903–2911.
39 B. W. An, E. J. Gwak, K. Kim, Y. C. Kim, J. Jang, J. Y. Kim and J. U. Park, *Nano Lett.*, 2016, **16**, 471–478.
40 D. J. Lipomi, J. A. Lee, M. Vosgueritchian, B. C. K. Tee, J. A. Bolander and Z. Bao, *Chem. Mater.*, 2012, **24**, 373–382.
41 D. Gupta, M. M. Wienk and R. A. J. Janssen, *Adv. Energy Mater.*, 2013, **3**, 782–787.

 

42 E. Dauzon, Y. Lin, H. Faber, E. Yengel, X. Sallenave, C. Plesse, F. Goubard, A. Amassian and T. D. Anthopoulos, *Adv. Funct. Mater.*, 2020, **30**, 2001251.
43 X. Fan, W. Y. Nie, S. H. Tsai, N. X. Wang, H. H. Huang, Y. J. Cheng, R. J. Wen, L. J. Ma, F. Yan and Y. G. Xia, *Adv. Sci.*, 2019, **6**, 1900813.
44 L. V. Kayser and D. J. Lipomi, *Adv. Mater.*, 2019, **31**, 1806133.
45 Y. Han, Z. Hu, W. Zha, X. Chen, L. Yin, J. Guo, Z. Li, Q. Luo, W. Su and C.-Q. Ma, *Adv. Mater.*, 2022, **34**, 2110276.
46 B. Y. Wang, T. H. Yoo, J. W. Lim, B. I. Sang, D. S. Lim, W. K. Choi, D. K. Hwang and Y. J. Oh, *Small*, 2015, **11**, 1905–1911.
47 Y. Sun, M. Chang, L. Meng, X. Wan, H. Gao, Y. Zhang, K. Zhao, Z. Sun, C. Li, S. Liu, H. Wang, J. Liang and Y. Chen, *Nat. Electron.*, 2019, **2**, 513–520.
48 Z. Liu, P. You, C. Xie, G. Tang and F. Yan, *Nano Energy*, 2016, **28**, 151–157.
49 S. Wageh, M. Raïssi, T. Berthelot, M. Laurent, D. Rousseau, A. M. Abusorrah, O. A. Al-Hartomy and A. A. Al-Ghamdi, *Sci. Rep.*, 2021, **11**, 14212.
50 H. Shi, C. C. Liu, Q. L. Jiang and J. K. Xu, *Adv. Electron. Mater.*, 2015, **1**, 1500017.
51 D. A. Mengistie, M. A. Ibrahem, P.-C. Wang and C.-W. Chu, *ACS Appl. Mater. Interfaces*, 2014, **6**, 2292–2299.
52 W. Meng, R. Ge, Z. Li, J. Tong, T. Liu, Q. Zhao, S. Xiong, F. Jiang, L. Mao and Y. Zhou, *ACS Appl. Mater. Interfaces*, 2015, **7**, 14089–14094.
53 M. Vosgueritchian, D. J. Lipomi and Z. Bao, *Adv. Funct. Mater.*, 2012, **22**, 421–428.
54 J. H. Lee, J. H. Heo, S. H. Im and O. O. Park, *ACS Appl. Mater. Interfaces*, 2020, **12**, 10527–10534.
55 X. Fan, B. Xu, S. Liu, C. Cui, J. Wang and F. Yan, *ACS Appl. Mater. Interfaces*, 2016, **8**, 14029–14036.
56 C. J. Brennan, J. Nguyen, E. T. Yu and N. S. Lu, *Adv. Mater. Interfaces*, 2015, **2**, 1500176.
57 V. Nicolosi, M. Chhowalla, M. G. Kanatzidis, M. S. Strano and J. N. Coleman, *Science*, 2013, **340**, 1226419.
58 S. R. Dupont, E. Voroshazi, D. Nordlund, K. Vandewal and R. H. Dauskardt, *Adv. Mater. Interfaces*, 2014, **1**, 1400135.
59 J.-W. Lee, C. Sun, D. J. Kim, M. Y. Ha, D. Han, J. S. Park, C. Wang, W. B. Lee, S. K. Kwon, T. S. Kim, Y. H. Kim and B. J. Kim, *ACS Nano*, 2021, **15**, 19970–19980.
60 L. Daelemans, W. Van Paepegem, D. R. D'hooge and K. De Clerck, *Adv. Funct. Mater.*, 2019, **29**, 1807434.
61 J. S. Park, G.-U. Kim, S. Lee, J.-W. Lee, S. Li, J.-Y. Lee and B. J. Kim, *Adv. Mater.*, 2022, **34**, 2201623.
62 J. Wan, X. Fan, H. Huang, J. Wang, Z. Zhang, J. Fang and F. Yan, *J. Mater. Chem. A*, 2020, **8**, 21007–21015.
63 J. Wan, Y. Xia, J. Fang, Z. Zhang, B. Xu, J. Wang, L. Ai, W. Song, K. N. Hui, X. Fan and Y. Li, *Nano-Micro Lett.*, 2021, **13**, 44.
64 N. Kim, S. Kee, S. H. Lee, B. H. Lee, Y. H. Kahng, Y.-R. Jo, B.-J. Kim and K. Lee, *Adv. Mater.*, 2014, **26**, 2268–2272.
65 B. J. Worfolk, S. C. Andrews, S. Park, J. Reinspach, N. Liu, M. F. Toney, S. C. B. Mannsfeld and Z. Bao, *Proc. Natl. Acacd. Sci. U. S. A.*, 2015, **112**, 14138–14143.
66 C. Bruner, F. Novoa, S. Dupont and R. Dauskardt, *ACS Appl. Mater. Interfaces*, 2014, **6**, 21474–21483.
67 Q. D. Yang, M. D. Thoules and S. M. Ward, *J. Adhes.*, 2000, **72**, 115–132.
68 J. P. Thomas, L. Zhao, M. Abd-Ellah, N. F. Heinig and K. T. Leung, *Anal. Chem.*, 2013, **85**, 6840–6845.
69 S. Y. Kim, Y. Kim, C. Cho, H. Choi, H. W. Park, D. Lee, E. Heo, S. Park, H. Lee and D. H. Kim, *ACS Appl. Mater. Interfaces*, 2019, **11**, 29350–29359.
70 K. R. Shull, K. I. Winey, E. L. Thomas and E. J. Kramer, *Macromolecules*, 1991, **24**, 2748–2751.
71 J. Noh, G.-U. Kim, S. Han, S. J. Oh, Y. Jeon, D. Jeong, S. W. Kim, T.-S. Kim, B. J. Kim and J.-Y. Lee, *ACS Energy Lett.*, 2021, **6**, 2512–2518.
72 J. Yuan, Y. Q. Zhang, L. Y. Zhou, G. C. Zhang, H. L. Yip, T. K. Lau, X. H. Lu, C. Zhu, H. J. Peng, P. A. Johnson, M. Leclerc, Y. Cao, J. Ulanski, Y. F. Li and Y. P. Zou, *Joule*, 2019, **3**, 1140–1151.
73 L. L. Zhan, S. X. Li, T. K. Lau, Y. Cui, X. H. Lu, M. M. Shi, C. Z. Li, H. Y. Li, J. H. Hou and H. Z. Chen, *Energy Environ. Sci.*, 2020, **13**, 635–645.
74 J. Seo, C. Kim, B. S. Ma, T. I. Lee, J. H. Bong, J. G. Oh, B. J. Cho and T. S. Kim, *Adv. Funct. Mater.*, 2018, **28**, 1806732.
75 J. C. Yang, S. Lee, B. S. Ma, J. Kim, M. Song, S. Y. Kim, D. W. Kim, T. S. Kim and S. Park, *Sci. Adv.*, 2022, **8**, eabn3863.
76 F. Greco, A. Zucca, S. Taccola, A. Menciassi, T. Fujie, H. Haniuda, S. Takeoka, P. Dario and V. Mattoli, *Soft Matter*, 2011, **7**, 10642–10650.
77 Y. H. Lee, B. K. Kang, H. D. Kim, H. J. Yoo, J. S. Kim, J. H. Huh, Y. J. Jung and D. J. Lee, *Macromol. Res.*, 2009, **17**, 616–622.
78 S. Kang, T. Yoon, S. Kim and T. S. Kim, *ACS Appl. Nano Mater.*, 2019, **2**, 1980–1985.